İSTANBUL UNIVERSITY CERRAHPAŞA

ORIGINAL ARTICLE
Electrica 2022; 22(1): 84-91

Using a Turn of a Meander Microstrip Line for ESD Protection

Roman S. Surovtsev[1,2], Alexander V. Nosov[2], Talgat R. Gazizov[1,2]

[1]Tomsk State University of Control Systems and Radioelectronics, Tomsk, Russian Federation
[2]Sirius University of Science and Technology, Sochi, Russian Federation

Cite this article as: R. S. Surovtsev, A. V. Nosov, T. R. Gazizov, "Using a Turn of a Meander Microstrip Line for ESD Protection," *Electrica*, 22(1), 84-91, Jan. 2022.

ABSTRACT

This article describes a new approach to electrostatic discharge (ESD) protection based on usage of a turn of a microstrip meander line (ML). The proposed approach enables decomposing an ESD peak surge with the duration of about 4 ns into a sequence of smaller amplitude pulses. Using a quasi-static simulation of the meander turn time response to the excitation of the IEC 61000-4-2 standard ESD current source, we obtained the condition for such decomposition. In addition, we derived the condition for the overlapping of the additionally reflected odd mode pulse of the negative polarity on the even mode pulse to reduce the amplitude of the last pulse. As an example, the proposed approach is used in investigating the ESD pulse propagation along the ML with various parameters. We also found the optimal value of the turn length for the minimum output ESD voltage, which decreases as the distance between the ML half-turns decreases. The described approach and the formulated conditions provide the improvement of the protection against ESD by decreasing its magnitude by several times. The effectiveness of the new approach is confirmed by the electrodynamic simulation and prototype measurements. The new research results supplement the theoretical framework for ESD mitigation techniques and can be used in designing reliable, light-weight, low-cost, and radiation-resistant ESD protection devices.
***Index Terms*—**Electrostatic discharge, even mode, meander line, odd mode, protective device.

I. INTRODUCTION

The urgent task of electromagnetic compatibility is to protect radio communications equipment (RCE) against various electromagnetic interferences (EMI). Electrostatic discharge (ESD) poses a great danger because it is capable of exerting negative influence on critical RCE and disabling it. Various approaches are used for RCE protection, although they are often inapplicable because of their complexity, costliness, or unreliability [1]. Meanwhile, for the uninterrupted operation of critical RCE, it is necessary to provide proper protection against ESD. Therefore, it is necessary to investigate new and simple protection approaches.

There are many devices for protecting RCE against ultra wideband (UWB) and ESD pulses that are well-characterized. For example, the paper [2] describes a systematic method to determine the protection capability of protection elements and the prediction of threshold levels in complex systems. The paper [3] presents the results of simulating, designing, and testing the interdigital bandpass filter types suitable for protecting electronic circuits against very fast transients of significant amplitude. The paper [4] discusses the possibility of SPICE simulations of common protection elements against extremely fast high-voltage UWB pulses. The paper [5] analyzes the waffle layout silicon-controlled rectifier-based ESD protection device. The paper [6] presents a new optimization method of ESD protection design, which uses a mixed-mode ESD simulation with a calibrated model based on DC and transmission line pulsing characteristics. The paper [7] demonstrates effective protection of power lines and low-frequency transmission lines with linear filters against UWB pulses.

Recently, interest has increased in the possibility of using coupled transmission lines in RCE as protective devices. The advantages of coupled transmission lines include simplicity of design, reliability, low cost, possibility of automated production, practically unlimited service life, and operation in a wide range of voltages. New coupled line protectors include modal filters (MFs) based on modal distortion [8]. Research into the MF technology is carried out in three main areas. The first involves the realization of MFs in printed circuit boards. Modal filters with different design features have been investigated and manufactured, for example, a reflection

Corresponding Author:
Alexander V. Nosov

E-mail:
alexns2094@tu.tusur.ru or alexns2094@gmail.com

Received: June 3, 2021

Accepted: August 23, 2021

Available Online Date: September 27, 2021

DOI: 10.5152/electrica.2021.21062

symmetric MF [9], an MF with a periodic profile of the conductor coupling region [10], a simple asymmetric MF [11], an MF with the passive conductor in the cutout of the reference plane [12], and an MF with the partially removed reference conductors [13]. The second research area is focused on MFs in the form of cables. The existing three-wire power cables of flat and round cross-sections were investigated [14]. In [15], the results of modeling and optimization of multi-wire MFs with a circular cross-section are presented: four structures of two to five conductors are considered. The third research area is modal reservation, the first results of which are systematized in [16].

Recently, a new technique for protecting RCE against UWB pulses has been proposed. It is based on the decomposition of a UWB pulse in the turn of a meander line (ML) into a sequence of pulses of smaller amplitude [17]. However, the application of this approach to the protection against ESD is understudied. In [18], the researchers examined the possibility of ESD decomposition in a turn of a meander microstrip line (MSL). They also presented the preliminary analysis results of how the ESD waveform and amplitude change as the length of the line increases. The results demonstrated that the ESD peak surge can be attenuated by 1.33 times by its decomposition. However, there are no studies investigating the possibility of additional attenuation of the ESD amplitude. The aim of this article is to fill this gap.

II. PROPOSED METHOD AND THEORETICAL BACKGROUND

The use of MLs for UWB protection is a new direction of research. The advantages of ML are the same as those of the MF, but the principle of protection is slightly different. The UWB can be decomposed in the ML into a sequence of two or three pulses of lower amplitude: into two pulses in the line with a homogeneous dielectric filling [19] and into three pulses—with an inhomogeneous filling [17]. The first pulse in both cases is the near-end crosstalk. In the line with a homogeneous dielectric filling, the second pulse is the sum of the odd and even modes. In the line with an inhomogeneous dielectric filling, the second and third pulses are the pulses of the odd and even modes, respectively. This difference is caused by the fact that in the line with a homogeneous dielectric filling, the propagation velocities of the even and odd modes are equal, while in the line with an inhomogeneous dielectric filling they are different. With this in mind, and knowing the ML length and the UWB duration, conditions were formulated, the fulfillment of which ensures such an expansion [17,19]. Another important condition is the optimal coupling between the ML half-turns. Its optimal value allows equalizing the amplitudes of all decomposed pulses and reducing the total amplitude at the ML output [17,19]. When designing protection devices, one of the important characteristics is its attenuation of interference pulse. To increase the UWB attenuation, multistage MLs were proposed [20]. The principle of such protection is similar to that described above in this section. However, first, it is necessary to decompose the UWB in the first turn into three pulses and then each of them in the second turn. As a result, the attenuation and the number of decomposition pulses at the output of the device increase. Another notable structure is an asymmetrical ML [21]. In this structure, the number of decomposition pulses and the UWB attenuation increase because of the appearance of the additional pulses arising from asymmetry. Finally, the UWB attenuation in hybrid protection devices based on ML and MF was demonstrated [22].

Note that the ESD waveform differs from the UWB waveform used in the above studies. In addition, the duration of the ESD is much longer than that of the UWB. However, an ESD peak surge has short duration and rise time and large amplitude. All this is dangerous for the RCE. The above-mentioned methods used to decompose a UWB pulse can be easily applied to decompose an ESD peak surge. But to begin with, it is advisable to use a simple and field-tested structure of the ML from [17]. Previously, the effect of length on the ESD decomposition in such a line was investigated [18]. However, the possibility of decreasing the amplitude by changing the optimal coupling between the conductors has not been investigated. In addition, because of the specific form of ESD (first fast and second slow falls), its amplitude can be further minimized. For example, it can be achieved by optimizing the cross-section parameters by means of increasing the coupling between the half-turns.

Therefore, we should summarize the obtained and propose the new results. For this, we need to analyze the change of the ESD waveform in a turn of a meander MSL with the change of its length to identify the optimal length of the half-turn for ESD peak decomposition, to investigate the possibilities of additional ESD attenuation, and to summarize the propagation of useful signals through the turn.

Initial geometrical and electrical parameters of the line are shown in Fig. 1. Excitation is the ESD current source chosen according to IEC 61000-4-2. Fig. 1 shows the voltage waveform at the beginning of a turn with a half-turn length (l) of 0.1 m and $R1 = R2 = 50\ \Omega$.

Complete ESD decomposition in the considered line will be at $l = 66$ m, though it is impractical [18]. However, we can decompose the ESD peak surge with the duration of about 4 ns rather than the whole ESD, providing the condition [18]

$$2l\left|\tau_e - \tau_o\right| \approx 4\ \text{ns} \quad (1)$$

where τ_e, τ_o are the per-unit-length delays of even and odd modes ($\tau_e = 6.66$ ns/m and $\tau_o = 5.9$ ns/m). From (1), it follows that for the ESD peak surge decomposition, it is sufficient to provide $l_{opt} = 2.63$ m.

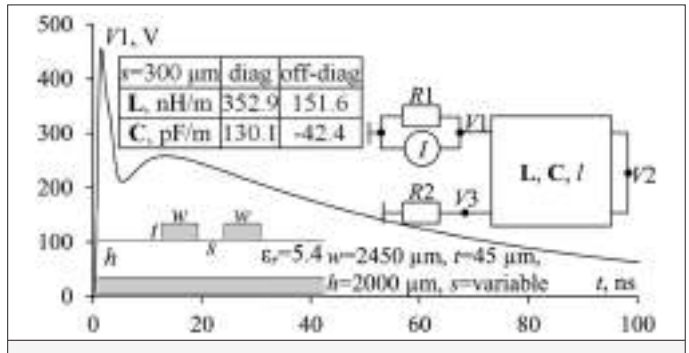

Fig. 1. $V1(t)$ for $l = 0.1$ m with cross-section, parameters, and circuit diagram under simulation.

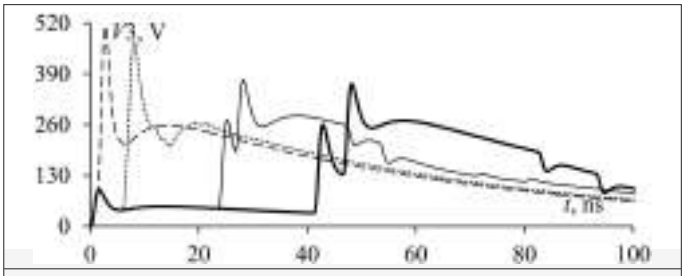

Fig. 2. *V*3(*t*) for *l* = 0.1 (– –), 0.5 (- -), 2 (––), 3.5 (▬) m for *s* = 300 μm.

The method of moments is widely used and proved to be good for simulating meander delay lines [23,24]. The simulation was performed using the TALGAT system [25], which implements the calculation of transmission line parameter matrices with the method of moments and the time response with the node-potential method [26]. The performed comparisons with other systems showed satisfactory coincidence of the results and the relevance of the TALGAT system for computing per-unit-length matrices for structures of various complexities [27]. There also exist indicative and commonly available examples comparing the TALGAT system results with the measurement [17,28] and electromagnetic analysis [29] results.

III. SIMULATION RESULTS

To understand the change of the ESD waveform in the ML turn, a detailed simulation with a sequential increase of *l* from 0.1 m to 10 m was performed. To name a few, the output voltage waveforms for *l* = 0.1, 0.5, 2, 3.5 m are shown in Fig. 2.

One can see the appearance of a crosstalk pulse (pulse 1) and also an increase of the main signal delay with the increase of the line length. We can see a slight increase (by 1.1 times for *l* = 0.1 m) of the signal amplitude at the end of the turn relative to the beginning. This is caused by the overlapping of the peak surge, which propagates through the turn on the near-end crosstalk from the surge. When the line length increases up to 3.5 m, pulses 2 and 3 (odd and even modes) are clearly exhibited.

Fig. 3 shows the dependence of the output voltage amplitude ($V3_{max}$) on *l*. It can be seen that a significant decrease of $V3_{max}$ is observed up to *l* = 2 m, whereas a further increase of *l* to 3 m produces only a slight effect. Thus, the increase of *l* by more than l_{opt} is inexpedient as it does not lead to a significant $V3_{max}$ decrease. In fact, it can even increase with the length increase to 4–6 m because of the last pulse (even mode) peak, which passes through the flat maximum of the previous pulse (odd mode). Herewith the feebly marked maximum is obtained for *l* = 5 m in Fig. 3.

A decrease of *s* leads to the increase of the crosstalk pulse amplitude and to the decrease of the odd and even mode pulse amplitudes [17]. A similar simulation was performed for *l* = 3 m but with a decrease of *s* from 300 to 1 μm. Fig. 4 shows the dependences of the amplitude of the first three signal peaks (crosstalk, odd mode, and even mode) on *s*. It can be seen that when *s* decreases, the odd and even mode amplitudes decrease, and the crosstalk amplitude increases. When *s* = 1 μm, they are aligned (about 100 V). Fig. 7 shows examples of *V*3(*t*) for *s* = 250, 150, 50, 10, 1 μm. It can be seen that the arrival times of peaks 1 and 3 do not change with the decrease of *s*, while peak 2 comes earlier because of the decrease of τ_o. Fig. 5 illustrates this where the dependences of τ_o and τ_e, and their differences ($\Delta\tau$) on *s* are given. The values of *R*1 and *R*2 for all simulations in which *s* is changed are set to be equal to $(Z_eZ_o)^{0.5}$. To illustrate this, the dependences of Z_o, Z_e, and $(Z_eZ_o)^{0.5}$ on *s* are shown in Fig. 6.

It is important to note that with the decrease of *s*, the delay of pulse 4 decreases (the odd-mode pulse, which is additionally reflected and has a negative polarity). Thus, for *s* = 1 μm, partial overlapping of the fall of pulse 3 and the front of pulse 4 is observed (Fig. 7).

As a result, with the further increase of the coupling between the conductors, the pulse 3 amplitude could be reduced because of its overlapping on pulse 4. However, to achieve this result, it is necessary to change the parameters of the line cross-section. This is important because a further decrease of the *s* parameter only (to increase the coupling between the conductors) is difficult to implement in practice. Obviously, the pulses will overlap if their delays are equal:

$$\tau_{max}\,2l = \tau_{min}\,4l, \Rightarrow \tau_{max} = 2\tau_{min} \quad (2)$$

where τ_{min} and τ_{max} are, in general case, the maximum and minimum values of per-unit-length delays of even and odd modes.

Note that if the decrease of *s* is difficult, then (2) can be fulfilled at the expense of other parameters of the cross-section (*t*, *h*, ε_r, and *w*). Therefore, the implementation of such line in practice will be possible.

To validate the obtained results, the simulation was performed using various approaches. Fig. 8 shows *V*3(*t*) for *l* = 3 m and

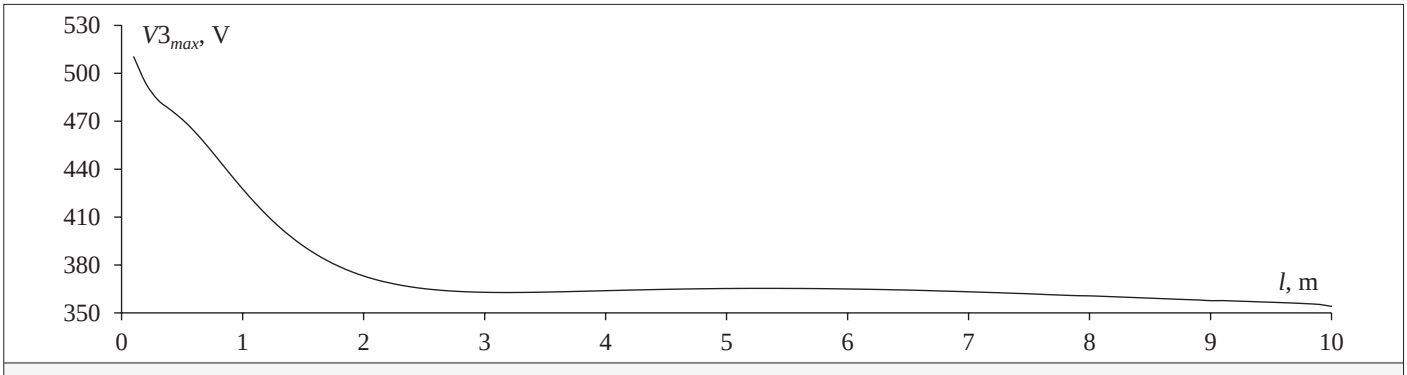

Fig. 3. $V3_{max}(l)$ for *s* = 300 μm.

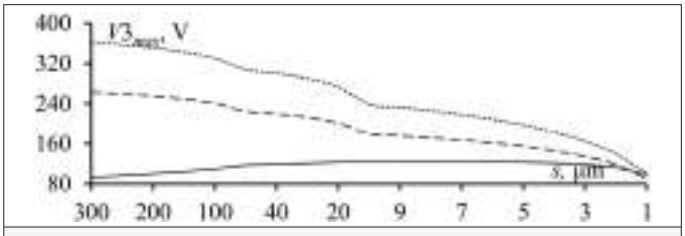

Fig. 4. $V3_{max}(s)$ of 1 (––), 2 (– –), and 3 (- -) peak amplitudes for $l = 3$ m.

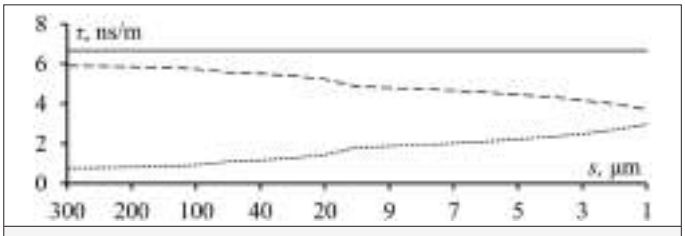

Fig. 5. Dependences τ_o (– –), τ_e (––) and $\Delta\tau$ (- -) on s.

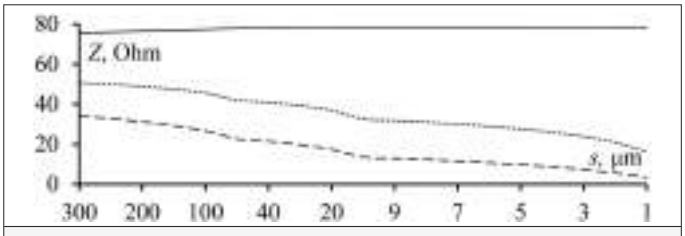

Fig. 6. Dependences Z_o (– –), Z_e (––), $(Z_eZ_o)^{0.5}$ (- -) on s.

$s = 300$ μm calculated using the quasistatic approach and the electrodynamic approach with coarse and fine meshes. Table I summarizes the amplitudes and delays of pulses 1–3. It can be seen that the voltage waveforms are in good agreement, and the differences are small (1–3%). It is also noteworthy that a finer mesh draws the results of the electrodynamic approach closer to the results of the quasistatic approach.

Previously, a slight increase of the signal amplitude was revealed at the turn output relative to the input for small values of l. For a more detailed analysis of this effect, the voltage amplitudes at the input and output of the turn were calculated for $s = 300$ μm and $l = 0$–0.2 m (Fig. 9). It can be seen that for $l = 0$–0.015 m, the voltage amplitudes at the input and output are almost the same (about 472 V). However, with a further increase of l, the voltage amplitude at the output increases up to 512 V (for $l = 0.1$ m) and then decreases to 495 V (at $l = 0.2$ m).

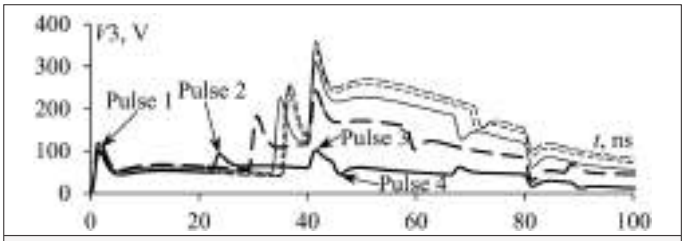

Fig. 7. $V3(t)$ for $l = 3$ m and $s = 250$ (– –), 150 (- -), 50 (––), 10 (▬ ▬), 1 (▬) μm.

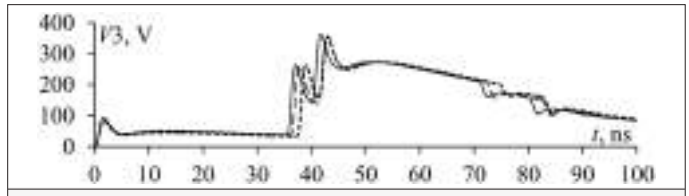

Fig. 8. $V3(t)$ for $l = 3$ m and $s = 300$ μm obtained using the quasistatic approach (––) and electrodynamic approach, with a coarse (- -) and fine (– –) mesh.

TABLE I. AMPLITUDES AND DELAYS OF THE OUTPUT PULSES CALCULATED USING VARIOUS APPROACHES

Approach	t_2, ns	t_3, ns	$V3_1$, V	$V3_2$, V	$V3_3$, V
Quasistatic	35.42	40.11	92.67	262.72	362.73
Electrodynamic (coarse mesh)	37.16	41.32	84.12	262.19	354.15
Electrodynamic (fine mesh)	35.96	41.05	94.01	261.64	358.82

At the same time, the voltage amplitude at the turn input decreases to 444 V at $l = 0.08$ m and then returns to 472 V. In this regard, when estimating the ratio of the input and output voltage amplitudes, it is critical to be precise. However, more important is the fact that there is a small region of l in which the output voltage is not attenuated but, on the contrary, increases. Therefore, it is necessary to investigate such dependencies in more detail.

It is obvious that the dependence of $V_{3max}(l)$ in Fig. 3 is non-monotonic and may have several extremes. Indeed, Fig. 3 shows the minimum and the weakly expressed maximum on the right, while the maximum in Fig. 9 is on the left of this minimum. Meanwhile, the behavior of $V3_{max}(l)$ may depend on other parameters. Examples for different values of s are shown in Fig. 10. We can see a strongly pronounced maximum at small l values. However, when s decreases to 1 μm, it practically disappears. In this case, the minimum and the second maximum become more pronounced and move to the region of smaller l values. This means the possibility of high attenuation at much lower values of l. The results in Fig. 10 were obtained, as before, for $R1 = R2 = (Z_eZ_o)^{0.5}$.

IV. EXPERIMENTAL RESULTS

Finally, we consider the effect of a turn on the distortion of useful signals. The effect on the power supply circuits will be negligible. The

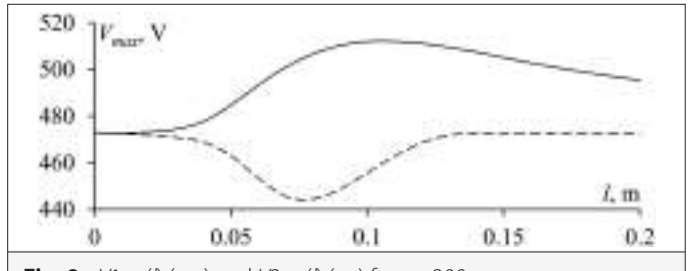

Fig. 9. $V1_{max}(l)$ (– –) and $V3_{max}(l)$ (––) for $s = 300$ μm.

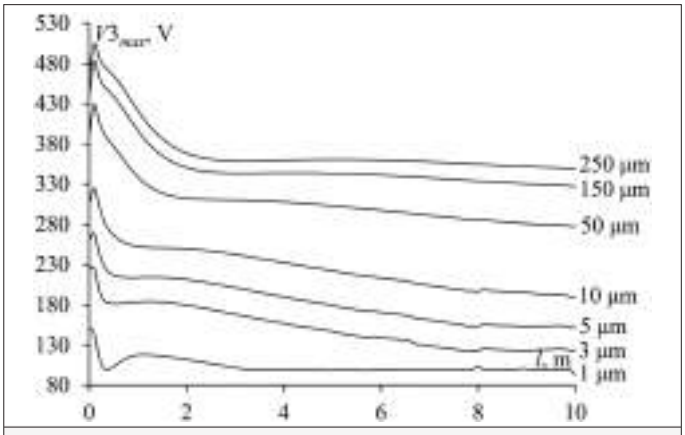

Fig. 10. $V3_{max}(l)$ for $s = 250$, 150, 50, 10, 5, 3, and 1 μm.

only drawback may be a small cross-section area of the conductor for a given current, which could be easily taken into account.

Previously, frequency dependences of $|S_{21}|$ for the turn prototypes have been measured [17]. Their passband is 1.1 GHz. Fig. 11 shows the frequency dependence of $|S_{21}|$ for the meander MSL prototype with $s = 150$ μm and $l = 90$ mm from [17]. It can be seen that useful signals with an upper boundary frequency up to 1.1 GHz will propagate through the turn with minimal amplitude distortions. To transmit the useful signals with a wider spectrum, the parameters of the turn should be optimized according to a number of criteria including the boundary frequency. However, the ESD spectrum is considerably attenuated at multiple minimums of the frequency dependence of $|S_{21}|$ observed at higher frequencies. They are caused by the fact that different components of a signal, at the same frequency, come to the ML output with different phases and compensate each other.

Next, we carried out full-scale tests (experiments) of the useful signal propagation through the prototypes from [17]. Before manufacturing the prototype of the line, the parameters of its cross-section were optimized. The optimization was performed according to the criteria of UWB decomposition and ensured the 50 Ω geometric mean of the characteristic impedance of the even and odd ML modes. The optimization also took into account the technological capabilities of the printed circuit board manufacturer. Then, the SMA (SubMiniature version A) connectors were soldered onto the input and output of the line.

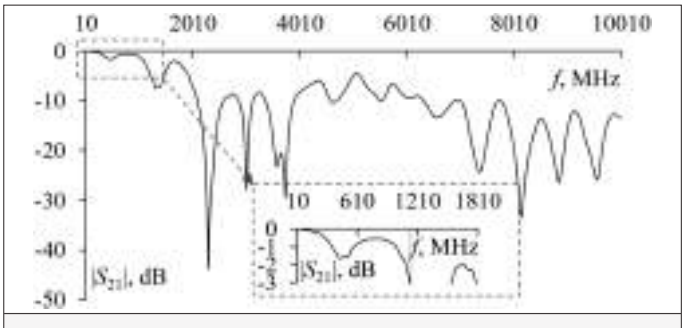

Fig. 11. Measured frequency dependence of $|S_{21}|$ for the meander MSL prototype with $s = 150$ μm and $l = 90$ mm from [17].

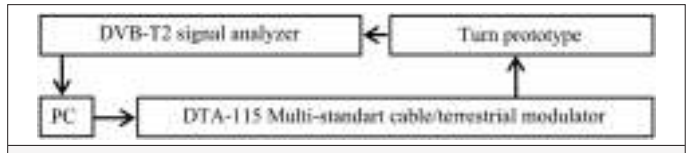

Fig. 12. System diagram of experimental setup.

We consider the TV signal of the DVB-T2 standard located in the frequency range of 48.5–862 MHz [30, 31]. Fig. 12 illustrates a system diagram of the experimental setup. DVB-T2 signal was formed with the established parameters using a DekTec DTA-115 GOLD multistandard modulator board connected to a PC via a peripheral component interconnect interface. The output impedance of the modulator board is 50 Ω. The MPEG transport system, with a capacity of 22,394,118 bps, was used as a traffic stream. First, to fix the frequency spectrum of the signal and its basic parameters such as signal level, modulation error ratio, and bit error ratio, the modulator board was directly connected to the signal analyzer Planar IT15-T2 by coaxial cable, which is connected to PC via a USB interface. The input impedance of the signal analyzer is 75 Ω. The ML prototype was connected to the measuring tract between the output of the modulator board and the input of the signal analyzer using a coaxial cable with BNC connectors at its ends. Cable impedance is 75 Ω. In the cable break, its ends are connected to the prototype terminals by soldering. The parameters of the signal transmitted by the modulator board were controlled using the DekTec StreamXpress software, and the signal reception and fixation of the parameters were controlled using the Planar ItToolsT2 software. The visual control of the image was carried out using a television receiver with an on-board DVB-T/T2 tuner. During the experiment, the signal parameters were first measured directly from the modulator board output. Then the ML prototype was connected between the output of the modulator board and the input of the signal analyzer.

Fig. 13 shows the measured voltage spectra in the frequency range of 45–900 MHz at the modulator output and the turn prototype outputs for carrier frequency (f_c) of 96 MHz. Obviously, the carrier propagates through the turn without a significant decrease. In the entire frequency range of the spectrum, there are interferences (no more than 16 dBμV) caused by external radiated emissions (possibly because the turn is not shielded).

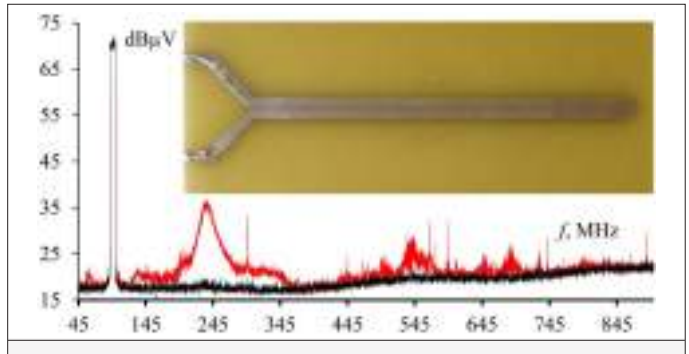

Fig. 13. Measured voltage spectra at the outputs of the modulator (▬) and the turn (▬) with a carrier frequency of 96 MHz, and photo of meander MSL prototype with $s = 150$ μm and $l = 90$ mm from [17].

Table II summarizes the levels of all channel signals and their differences. Therewith, a number of other parameters were controlled, including the signal constellations of QAM 64, which are not provided here.

When a signal propagates through the turn, its level slightly decreases relative to the signal at the modulator output. Thus, the maximum attenuation of the amplitude was 2.9 dBμV. The attenuation may be caused by inhomogeneities of connectors that connect the turn and the measuring path, by soldering coaxial cables to the turn terminals and by insufficient matching of the generator and load.

V. COMPARISON OF PROPOSED AND EXISTING SOLUTIONS

The proposed meander line approach has a number of advantages in comparison with traditional solutions for protecting the RCE against ESD. The first advantage is high speed. As the process of pulse decomposition starts with its propagation in the ML, it does not depend on the steepness of the front and the amplitude, as opposed to gas discharge devices. Another advantage is the absence of semiconductor components, as opposed to varistors and, as a consequence, high radiation resistance and high operating life cycle. Moreover, MLs are independent on the influence of parasitic inductances of leads, in contrast to transient voltage suppressor diodes. Finally, MLs are easy to design and cost effective.

ML also outperform MF as their most close solution. First, MLs provide additional attenuation thanks to an additional (near-end crosstalk) decomposition pulse. Then, an ML has a half-length structure due to the double-length propagation along the two half-turns. Finally, as MLs have no passive conductors, they do not need resistors.

VI. CONCLUSION

The main results of the article can be outlined in the following way:

- We have summarized the results of how the waveform and amplitude of an ESD after propagation along a turn of a meander MSL change with the increase of its length.

TABLE II. CARRIER LEVELS (DBμV) AT THE MODULATOR AND TURN OUTPUTS AND THEIR DIFFERENCE

f_c, MHz	U_M	U_T	U_M–U_T
96	70.8	69.6	1.2
202	70.9	68.9	2
298	70.3	67.4	2.9
402	68.9	68.2	0.7
498	69.7	67.6	2.1
602	68.9	67.6	1.3
698	69.8	68.3	1.5
802	69.4	68.0	1.4
850	68.3	65.6	2.7

- We have revealed the existence of the optimal value of the turn length for the minimum output ESD voltage. The fact is caused by specific behavior of the ESD waveform consisting of quick and slow parts.
- We have analyzed in detail the obtained values of the per-unit-length mode delays and voltage waveforms at the output of a meander MSL, when *s* is changed up to 1 μm. In addition, we formulated a condition that ensures the arrival of the odd mode pulse (reflected additionally from the far end of the line and having a negative polarity) at the time of the arrival of the even mode pulse. Thus, we have revealed the possibility for the voltage amplitude to additionally decrease at the line output. However, to correctly use such a possibility, it is necessary to equalize the amplitude of the third pulse with the amplitudes of the first and second pulses. This can only be achieved by using the reflections in the line (e.g., in the case of a line mismatch with the path in which it is used).
- We have presented the results of experimental studies of the propagation of a useful signal in an ML. The results show that the useful signal can propagate with ESD attenuation.
- The comparison of the proposed and existing solutions shows that existing advantages of ML can open suitable areas of their usage.

In this article, the simulation was performed without taking into account losses that can also affect the ESD waveform and amplitude at the ML output. This is planned for further research. We also note that the work demonstrated only an approach to protecting RCE against ESD by means of the MSL characteristics. In this regard, a large value of *l* or a small value of *s* can be easily changed in practice, while maintaining other parameters of the ML. For example, *s* can be increased along with a proportional increase of *h* and *t*. The dimensions of the device can be reduced by choosing a material with a higher ε_r or folding the original ML into several turns.

Peer-review: Externally peer-reviewed.

Author Contributions: Concept – T.R.G.; Design – R.S.S.; Supervision – R.S.S.; Materials – A.V.N.; Data Collection and/or Processing – A.V.N.; Analysis and/or Interpretation – A.V.N.; Literature Search – R.S.S.; Writing Manuscript – T.R.G.; Critical Review – T.R.G.

Acknowledgments: The authors thank the reviewers for their comments. The authors are with the Tomsk State University of Control Systems and Radioelectronics, 634050, Tomsk, Russia (e-mail: surovtsevrs@tu.tusur.ru; alexns2094@tu.tusur.ru; talgat@tu.tusur.ru).

Conflict of Interest: The authors have declared that no conflicts of interest exist.

Financial Disclosure: The research was supported by the Ministry of Science and Higher Education of the Russian Federation (Projects FEWM-2020-0041 and FEWM-2020-0039).

REFERENCES

1. Z. M. Gizatullin and R. M. Gizatullin, "Investigation of the immunity of computer equipment to the power-line electromagnetic interference," *J. Commun. Technol. Electron.*, vol. 61, no. 5, pp. 546–550, 2016. [CrossRef]

2. R. Krzikalla, J. Luiken, J. L. ter Haseborg and F. Sabat, "Systematic description of the protection capability of protection elements," in Proceedings of IEEE International Symposium on Electromagnetic Compatibility, Honolulu, USA, 2007, pp. 1–4.
3. R. Krzikalla, T. Weber and J. L. ter Haseborg, "Interdigital microstrip filters as protection devices against ultrawideband pulses," in Proceedings of IEEE International Symposium on Electromagnetic Compatibility, Istanbul, Turkey, 2003, pp. 1313–1316.
4. R. Krzikalla and J. L. ter Haseborg, "SPICE simulations of UWB pulse stressed protection elements against transient interferences," in Proceedings of IEEE International Symposium on Electromagnetic Compatibility, Chicago, USA, 2005, pp. 977–981.
5. Q. Cui, S. Dong and Y. Han, "Investigation of waffle structure SCR for electrostatic discharge (ESD) protection," in IEEE International Conference on Electron Devices and Solid State Circuit (EDSSC), Bangkok, Thailand, 2012, pp. 3–5.
6. H. Hayashi, T. Kuroda, K. Kato, K. Fukuda, S. Baba and Y. Fukuda, "ESD protection design optimization using a mixed-mode simulation and its impact on ESD protection design of power bus line resistance," in International Conference on Simulation of Semiconductor Processes and Devices (SISPAD), Tokyo, Japan, 2005, pp. 99–102.
7. T. Weber, R. Krzikalla and J. L. ter Haseborg, "Linear and nonlinear filters suppressing UWB pulses," *IEEE Trans. Electromagn. Compat.*, vol. 46, no. 3, pp. 423–430, 2004. [CrossRef]
8. A. T. Gazizov, A. M. Zabolotsky and O. A. Gazizova, "New printed structures for protection against UWB pulses," in 16th International Conference of Young Specialists on Micro/Nanotechnologies and Electron Devices (EDM), Erlagol, Russia, 2015, pp. 120–122.
9. E. S. Zhechev, E. B. Chernikova, A. O. Belousov and T. R. Gazizov, "Experimental research of a reflection symmetric modal filter in the time and frequency domains,"(in Russian), *Syst. Control. Commun. Sec.*, vol. 2, pp. 162–179, 2019. [CrossRef]
10. R. R. Khazhibekov, "Study of the amplitude-frequency characteristics of modal filters with a passive conductor in the form of a series of transmission line segments,"(in Russian), *Proceedings of Tomsk State University of Control Systems and Radioelectronics*, vol. 22, no. 2, pp. 31–36, 2019. [CrossRef]
11. A. T. Gazizov, A. M. Zabolotsky and T. R. Gazizov, "UWB pulse decomposition in simple printed structures," *IEEE Trans. Electromagn. Compat.*, vol. 58, no. 4, pp. 1136–1142, 2016. [CrossRef]
12. M. A. Samoylichenko, Y. S. Zhechev, V. P. Kosteletskii and T. R. Gazizov, "Electrical characteristics of a modal filter with a passive conductor in the reference plane cutout," *IEEE Trans. Electromagn. Compat.*, vol. 63, no. 2, pp. 435–442, 2021. [CrossRef]
13. M. A. Samoylichenko and T. R. Gazizov, "Parametric and structural optimization of the modal filter on a double-sided printed circuit board," *J. Phys. Conf. S.*, vol. 1862, no. 012020, pp. 1–7, 2021.
14. T. R. Gazizov and A. M. Zabolotsky, "Experimental results on UWB pulse propagation in low-voltage power cables with different cross sections, " *IEEE Trans. Electromagn. Compat.*, vol. 54, no. 1, pp. 229–231, 2012. [CrossRef]
15. A. O. Belousov and N. O. Vlasova, "Parametric optimization of the cables with the modal filtration effect, " *J. Phys. Conf. S.*, vol. 1862, no. 012020, pp. 1–5, 2021.
16. V. R. Sharafutdinov and T. R. Gazizov, "Analysis of the reservation methods with modal filtration base,"(in Russian), *Syst. Control. Commun. Sec.*, vol. 3, pp. 117–144, 2019. [CrossRef]
17. R. S. Surovtsev, A. V. Nosov, A. M. Zabolotsky and T. R. Gazizov, "Possibility of protection against UWB pulses based on a turn of a meander microstrip line," *IEEE Trans. Electromagn. Compat.*, vol. 59, no. 6, pp. 1864–1871, 2017. [CrossRef]
18. A. V. Nosov, R. S. Surovtsev and T. R. Gazizov, "Investigation of possibility of protection against electrostatic discharge using meander microstrip line," *J. Phys. Conf. S.*, vol. 1015, no. 2, pp. 1–6, 2018. [CrossRef]
19. R. S. Surovtsev, T. R. Gazizov and A. M. Zabolotsky, "Pulse decomposition in a turn of meander line as a new concept of protection against UWB pulses," in *Proceedings of Siberian Conference on Control and Communications (SIBCON)*, Omsk, Russian Federation, 2015, 5 p.
20. G. Y. Kim, A. V. Nosov, R. S. Surovtsev, T. T. Gazizov and A. E. Maximov, "Conditions for ultrashort pulse decomposition in multi-cascade protection devices based on meander microstrip lines, " *J. Phys. Conf. S.*, vol. 1679, no. 022059, pp. 1–6, 2020.
21. A. O. Belousov et al., "From symmetry to asymmetry: The use of additional pulses to improve protection against ultrashort pulses based on modal filtration," *Symmetry*, vol. 12(7), no. 1117, pp. 1–39, 2020.
22. A. V. Nosov, A. O. Belousov, R. S. Surovtsev and T. R. Gazizov, "Simulating hybrid protection against ultrashort pulse based on its modal decomposition," *J. Phys. Conf. S.*, vol. 1353, no. 012022, pp. 1–6, 2019. [CrossRef]
23. B. J. Rubin and B. Singh, "Study of meander line delay in circuit boards," *IEEE Trans. Microw. Theor. Tech.*, vol. 48, no. 9, pp. 1452–1460, 2000. [CrossRef]
24. A. U. Bhobe, C. L. Holloway and M. Piket-May, "Meander delay line challenge problems: A comparison using FDTD, FEM and MoM," in International Symposium on Electromagnetic Compatibility, 2001, pp. 805–810.
25. S. P. Kuksenko, "Preliminary results of TUSUR University project for design of spacecraft power distribution network: EMC simulation," *IOP Conf. S. Mater. Sci. Eng.*, vol. 560, pp. 1–7, 2019. [CrossRef]
26. J. R. Griffith and M. S. Nakhla, "Time-domain analysis of lossy coupled transmission lines," *IEEE Trans. Microw. Theor. Tech.*, vol. 38, no. 10, pp. 1480–1487, 1990. [CrossRef]
27. T. R. Gazizov, I.Ye. Sagiyeva and S. P. Kuksenko, "Solving the complexity problem in the electronics production process by reducing the sensitivity of transmission line characteristics to their parameter variations," *Complexity*, vol. 2019, pp. 1–11, 2019. [CrossRef]
28. A. T. Gazizov, A. M. Zabolotsky and T. R. Gazizov, "Measurement and simulation of time response of printed modal flters with broad-side coupling," *J. Commun. Technol. Electron.*, vol. 63, no. 3, pp. 270–276, 2018.
29. P. E. Orlov, T. R. Gazizov and A. M. Zabolotsky, "Short pulse propagation along microstrip meander delay lines with design constraints: Comparative analysis of the quasi-static and electromagnetic approaches," *Appl. Comp. Electromagn. Soc. J.*, vol. 31, no. 3, pp. 238–243, 2016.
30. *Digital Video Broadcasting (DVB)*, "Frame structure channel coding and modulation for a second generation digital terrestrial television broadcasting system (DVB–T2), ETSI EN 302 755 V1.1.1," 2009-09.
31. R. S. Surovtsev, V. V. Kapustin and A. V. Nosov, "Transmission of DVB-T2 standard signal in a turn of protective meander microstrip line," in International Siberian Conference on Control and Communications (SIBCON). Tomsk, Russia, 2019, p. 4.

Roman S. Surovtsev was born in 1991. He received an engineering degree and Ph.D. degree in radio engineering from Tomsk State University of Control Systems and Radioelectronics (TUSUR), Tomsk, Russia, in 2013 and 2016, accordingly. He is currently a senior researcher at TUSUR. He is the author and coauthor of 113 scientific papers.

Alexander V. Nosov was born in Semipalatinsk, Kazakhstan, in 1994. He received a bachelor's degree, master's degree, and Ph.D. degree in radio engineering from Tomsk State University of Control Systems and Radioelectronics (TUSUR), Tomsk, Russia, in 2015, in 2017, and in 2018, accordingly. Currently, he is working as a senior researcher at TUSUR. He is the author and coauthor of 57 scientific papers.

Talgat R. Gazizov was born in 1963. He received the engineering degree, Ph.D. degree, and Dr. Habil. of engineering sciences degree from Tomsk State University of Control Systems and Radioelectronics (TUSUR), Tomsk, Russia, in 1985, 1999, and 2010, respectively. His current research interests include signal integrity problem. He is the author or coauthor of 388 scientific papers.